Hindawi Publishing Corporation
Journal of Nanomaterials
Volume 2015, Article ID 418024, 8 pages
http://dx.doi.org/10.1155/2015/418024

*Research Article*

# The Influence of Thermal Conditions on $V_2O_5$ Nanostructures Prepared by Sol-Gel Method

**M. Prześniak-Welenc, M. Łapiński, T. Lewandowski, B. Kościelska, L. Wicikowski, and W. Sadowski**

*Faculty of Applied Physics and Mathematics, Gdańsk University of Technology, Narutowicza 11/12, 80-233 Gdańsk, Poland*

Correspondence should be addressed to M. Prześniak-Welenc; mprzesniak@mif.pg.gda.pl

Received 4 December 2014; Accepted 22 January 2015

Academic Editor: Wei-Chun Chen



This work presents the result of structure investigations of $V_2O_5$ nanorods grown from thin films and powders prepared by sol-gel method. To examine the best temperature of nanorods crystallization, thin films deposited by spin-coating method on quartz glass or silicon substrates and bulk xerogel powders were annealed at various temperatures ranging from 100°C to 600°C. The structure of the samples was characterized by X-ray diffraction method (XRD), scanning electron microscope (SEM), differential scanning calorimetry (DSC), thermogravimetric analysis (TGA), and mass spectroscopy (MS). The rod-like structure of $V_2O_5$ was obtained at 600°C on both quartz glass and silicon substrates and also from the bulk xerogel. The growth process and the effect of annealing treatment on the nanostructure are briefly discussed.

## 1. Introduction

For the last decade, one-dimensional (1D) nanostructures have been intensively studied due to their remarkable physical and chemical properties, which may predispose them to potential applications in highly functional devices [1]. Because of their fascinating physical and chemical properties, vanadium oxide nanostructures seem to be especially interesting. These result from the various metal oxidation states (from +II to +V) and the different V-O coordination geometries, which allows for many commercial applications in optical, electrical, electrochemical, and thermochromic devices [2–6]. The most stable oxide in the V-O system is $V_2O_5$ and has several polymorphs, including $\alpha$-$V_2O_5$ (orthorhombic) [7], $\beta$-$V_2O_5$ (monoclinic or tetragonal) [8], and $\gamma$-$V_2O_5$ (orthorhombic) [9]. The synthesized $V_2O_5$ nanomaterials compared to commercial materials appreciably improve the performance in devices for energy storage and photocatalytic. For instance, Pan et al. [10] reported that a nanostructured vanadium oxide ($V_2O_5$) exhibits much better electrochemical performance for high-rate lithium batteries than commercial microsized $V_2O_5$. Puangpetch et al. [11] showed that $V_2O_5$ nanosheet synthesized via surfactant modified sol-gel technique exhibited superior photocatalytic $H_2$ production activity than a commercially available $V_2O_5$ powder for both self-photoexcitation and dye photosensitization systems under visible light radiation.

Nanostructured 1D vanadium oxides are usually prepared by different techniques, as hydrothermal method, electrospinning, magnetron sputtering, controllable self-assembly, and sol-gel method [1, 6, 12]. The most favorable method for preparation of 1D structures may be sol-gel technique. It is due to its low cost and simple procedure [13]. The sol-gel method is based on the hydrolysis and condensation processes of molecular precursors, for instance, metal alkoxides or hydroxylated metal ions in aqueous solutions [14], and offers a suitable synthetic path for creating materials with very unusual properties as compared to traditional solid-state chemical techniques [15]. There are a lot of papers about $V_2O_5$ nano- and microstructures preparation by sol-gel technique. For instance, Gotić et al. [16] obtained $V_2O_5$ powders consisting of big particles of irregular shape using vanadium (V) triisopropoxide as a precursor. Özer [6] prepared $V_2O_5$ films by the spin-coating method used the same precursor in sol-gel method as Gotić. The main aim of his studies was electrochemical properties of amorphous and transparent $V_2O_5$ films. Additionally, Özer observed that, above 350°C, thin films were slightly crystalline. Vasanth Raj et al. [15]

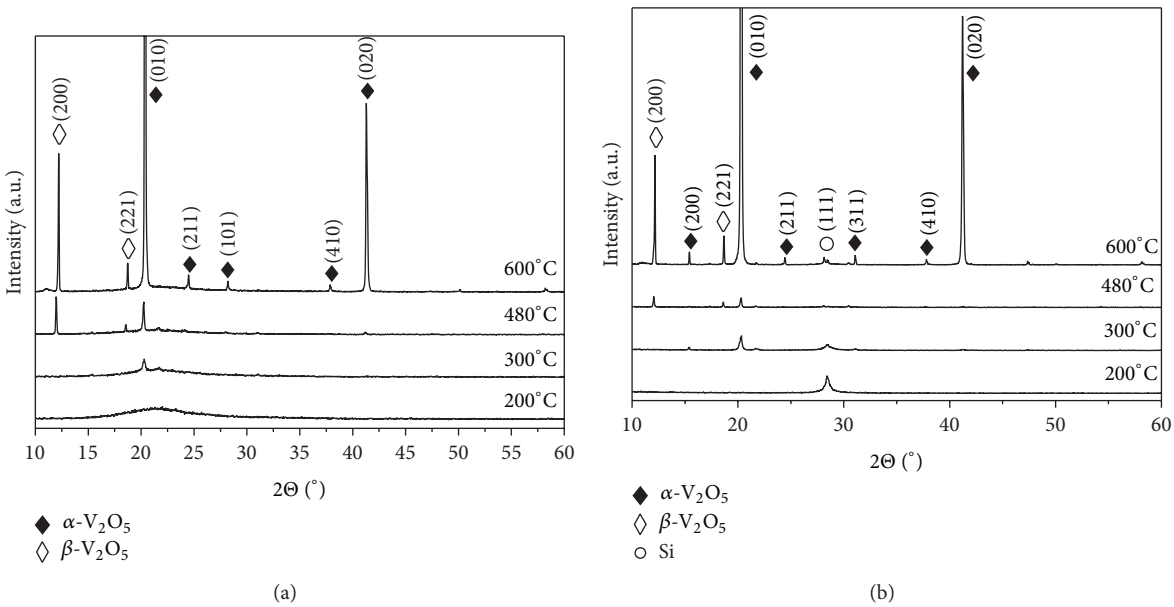


Figure 1: XRD patterns of coatings deposited on quartz glass (a) and silicon (b) after heat treatment for 10 h at various temperatures: 200°C, 300°C, 480°C, and 600°C.

described growth of one-dimensional $V_2O_5$ nanorods on glass substrates by a dip-coating process from a sol synthesized by sol-gel method using $V_2O_5$ powder as a precursor, whereas Niederberger et al. [17] prepared $V_2O_5$ nanorods from $VOCl_3$ sol. However, there is a lack of information about difference between the formation of $V_2O_5$ nanorods on the substrate surface and from the xerogel powder from the same precursor. Also the influence of the substrate structure on the nanorods growth is still considered in literature.

In the present work, we have focused on the synthesis and structure investigations of $V_2O_5$ nanorods grown on substrates and from xerogel powders. In both cases, the precursor was the same and nanorods were grown during thermal annealing.

## 2. Experimental

*2.1. Synthesis.* The starting solution was prepared by mixing vanadium (V) oxytripropoxide, an anhydrous ethyl alcohol as solvent and acetylacetone. The coatings were deposited by spin-coating technique at a rate of 100 rps on precleaned quartz glass and silicon substrates and dried at 50°C for 48 h in air atmosphere. After this, transparent and homogeneous coatings were obtained. Repeating the above procedure three times resulted in approximately 600 nm thick films. The thickness of the films was measured by Tencor Alpha-Step 500 stylus-based surface profiler. By drying the sol at the same conditions as thin films, it transforms via gel into a xerogel powder. To obtain nanocrystals, the films and the xerogel powders were subsequently annealed at the temperatures ranging from 100°C to 600°C for 10 h and then cooled to the room temperature.

*2.2. Characterization.* Phase composition of manufactured samples was examined by X-ray diffraction method (XRD) by Philips X'Pert diffractometer system using CuK$\alpha$ radiation in a range of 10°–80° of $2\theta$. Surface morphology of the samples was studied with scanning electron microscope (SEM) using FEI Company Quanta FEG 250. All measurements were carried out at room temperature.

Simultaneous thermogravimetric analysis (TGA) and differential scanning calorimetry (DSC) were performed under synthetic air with heating rate 10°C/min from 40°C to 700°C using Netzsch STA 449 F1. This system is characterized by a very high resolution, $25 \times 10^{-12}$ kg at a weighing range of $5 \times 10^{-3}$ kg. However, there are several uncertainties associated with TGA measurements. The STA449 F1 has a vertical sample carrier and in order to account for buoyancy effects, a correction curve with empty crucibles was first obtained and then subtracted from the experimental results. To avoid heat and mass transfer limitations, approximately $4 \times 10^{-6}$ kg of sample was used, and platinum/rhodium crucibles without lids were employed. The total uncertainty associated with measurement was 0.005% by weight of the sample and was included in the final result. The thermal behavior has been studied by using TGA with mass spectrum (MS). The gases that come out from sample during heating were monitored by the quadruple mass spectrometer Netzsch QMS 403C Aëolos. The FT-IR spectra were recorded at room temperature using Perkin-Elmer spectrometer (model Frontier FTIR MIR/FIR). The FT-IR spectra of the samples pressed into KBr pellets were collected in the wave number range 4000–400 $cm^{-1}$ (mid-IR region) using the KBr beam splitter.

## 3. Results and Discussion

Evaluation of the X-ray diffraction patterns of the coatings deposited on quartz glass and silicon substrate depending on annealing temperature is shown in Figures 1(a) and 1(b), respectively. The diffraction peaks of samples annealed at 600°C match very well the JCPDS Card number 089-0611

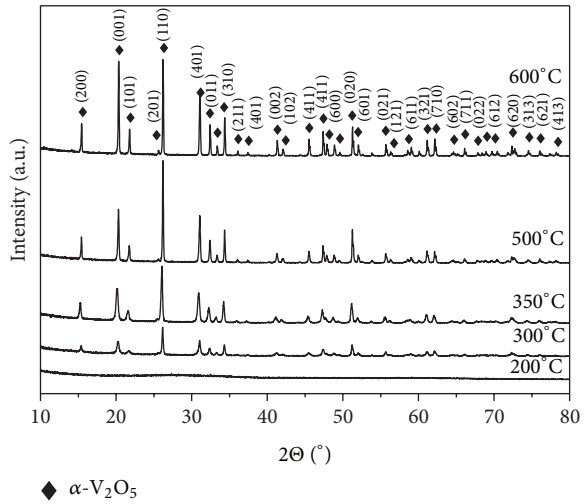


Figure 2: XRD patterns of the xerogel powders after heat treatment for 10 h at various temperatures: 200°C, 300°C, 350°C, 500°C, and 600°C.

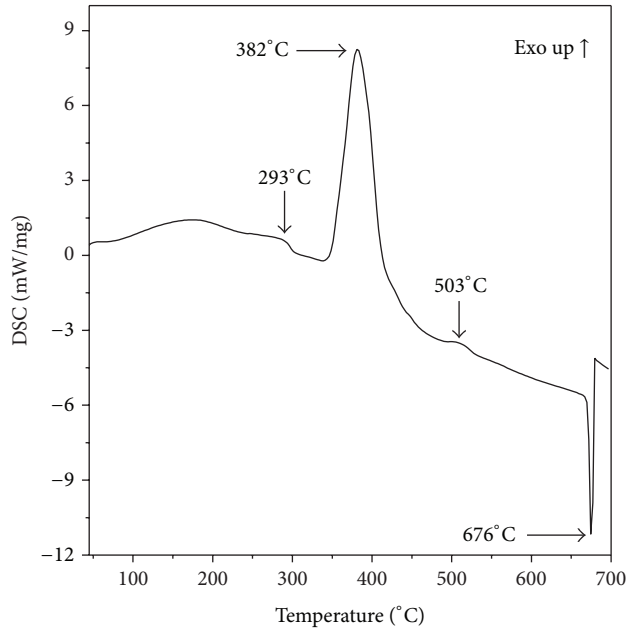


Figure 3: DSC curve of as-prepared xerogel powder in air.

which corresponds to the orthorhombic structure with a space group of Pmn (number 21).

The samples annealed at 200°C, 300°C, 480°C, and 600°C show significant structural changes. The crystallization process starts after heat treatments at 300°C and $\alpha$-$V_2O_5$ is the only crystalline phase in the films. Below this temperature, films are amorphous with visible characteristic peaks of substrates. After increasing the annealing temperature up to 480°C, a sharp peaks appeared in XRD patterns, indicating crystallization of $\beta$-$V_2O_5$ [8, 15, 18]. When the temperature rises to 600°C, reflections of $V_2O_5$ become more clearly defined. The patterns correspond to a mixture structure of $\alpha$-$V_2O_5$ and $\beta$-$V_2O_5$ phases. It may be seen that the films deposited on quartz glass and silicon (Figures 1(a) and 1(b), resp.) have preferential orientation along (010) plane.

Crystalline structures which were grown in thin films are also present, after heating in the same thermal conditions, in xerogel powders. XRD patterns of the powders heated at different temperatures are shown in Figure 2.

The diffraction peaks of the sample annealed at 600°C match very well the JCPDS Card number 41-1426, which corresponds to the orthorhombic structure with a space group of Pmmn (number 59). The crystallization process also starts after heat treatments at 300°C and $\alpha$-$V_2O_5$ is the only crystalline phase present in the sample. XRD patterns reveal that the intensity of diffraction peaks of $\alpha$-$V_2O_5$ increases when the temperature rises up to 600°C. Further, no signals of other $V_2O_5$ phases were detected, indicating that high purity of $\alpha$-$V_2O_5$ product was obtained. In comparison, thin films deposited on both substrates and annealed at 600°C exhibit mixture structure of $\alpha$-$V_2O_5$ and $\beta$-$V_2O_5$ phases, whereas powder annealed at this same temperature exhibits pure orthorhombic phase ($\alpha$-$V_2O_5$).

The crystallite size of the $V_2O_5$ nanoparticles was calculated by the X-ray line broadening method using the Scherrer equation:

$$D = \frac{k\lambda}{\beta_{hkl} \cos\theta}, \quad (1)$$

where $D$ is the crystallite size, $\lambda$ the Cu $K_\alpha$ radiation of wavelength (1.5406 Å), $k$ the shape factor (0.9), $\beta_{hkl}$ the full width at half maximum (FWHM) in radian, and $\theta$ the scattering angle. The average crystallite size of the thin films deposited on both substrates was calculated to the (110) plane of $\alpha$-$V_2O_5$ diffraction peak. Crystallite sizes in these samples annealed at 300°C, 480°C, and 600°C were, respectively, about 40 nm, 80 nm, and 150 nm independent of the used substrate type. For other planes of diffraction peaks, the Scherrer formula cannot be used because the diffraction peaks are too narrow and calculated crystallite size was above 1 $\mu$m. In the case of powders, the average crystallite size was calculated to the most intensive peak corresponding to the (110) plane. The crystallite sizes for these samples annealed at 300°C, 350°C, 500°C, and 600°C were, respectively, about 60 nm, 80 nm, 350 nm, and 350 nm.

Figure 3 shows differential scanning calorimetry (DSC) results for as-prepared xerogel powder. DSC spectra show three exothermic peaks at 293°C, 382°C, and 503°C and one endothermic peak at 676°C. It may be noticed on the basis of the thermal analysis results and the study of XRD patterns that the first exothermic peak located at 293°C in the DSC curve can be attributed to the beginning of the crystallization process of $\alpha$-$V_2O_5$. The next one at 382°C may correspond to $\alpha$-$V_2O_5$ structure transformation: $\alpha$-$V_2O_5$ nanocrystals start to form $\alpha$-$V_2O_5$ nanorods. With this process, the mass losses of the sample are correlated (see Figure 4). Evaporation of residual organics probably predisposes to crystallization process of nanorods. Exothermic peak at 503°C may be attributed to $\beta$-$V_2O_5$ phase formation. This phase is not observed in XRD results. However, the quantity of this phase may be too little to be detected by our equipment. On the other hand, $\beta$-$V_2O_5$ phase is not stable and could transform into $\alpha$-$V_2O_5$

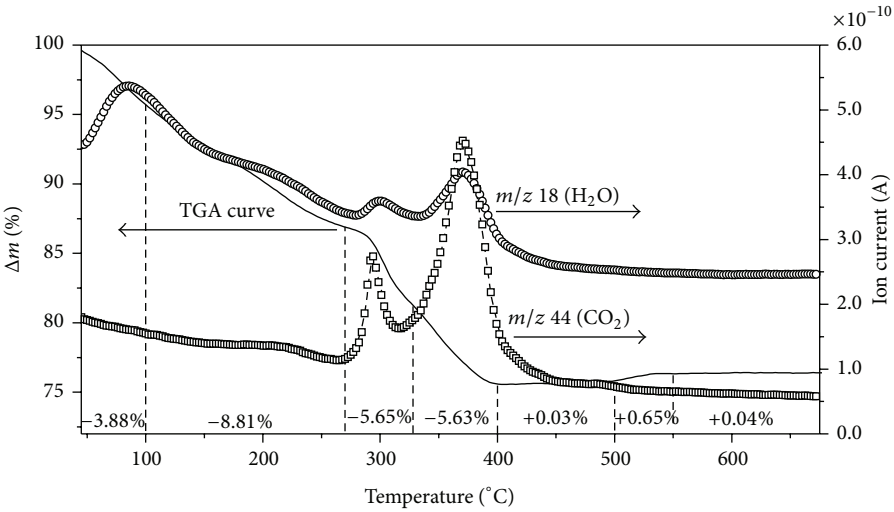


Figure 4: TGA curve with in situ mass spectrum of xerogel powder in the flow of oxygen.

phase during cooling. The transition process ($\alpha$-$\beta$) is connected with compression of structure along the $c$-axis by crystallographic shear [9]. In the case of $V_2O_5$ thin films, the substrates (silicon and quartz glass) support the formation of isolated $VO_x$ units containing one terminal V=O bond and three bridging V–O–Si bonds (trigonal pyramidal coordinations) [19]. The interaction between a substrate surface and vanadium oxide thin films stabilizes the structure and prevents transformation $\beta$-$V_2O_5$ into $\alpha$-$V_2O_5$ phase during cooling.

A sharp endothermic peak at 676°C is due to the melting of $V_2O_5$. The melting temperature is in good agreement with reported data [20, 21].

TGA with MS is a power method to analyze the mechanism of thermal behavior of the samples. The abundance of the $m/z$ 18 and $m/z$ 44 signals versus temperature can be seen in Figure 4. The $m/z$ 18 signal corresponds to the ($H_2O$), and the $m/z$ 44 signal corresponds to ($CO_2$). The peak of $m/z$ 18 below 100°C suggests that the weight loss of 3.88% in the TGA curve is due to the evaporation of water from the sample surface. The broad peak on the mass spectrum of $m/z$ 18 observed between 150°C and 270°C indicates that the abrupt weight loss of 8.81% from 100°C to 270°C period corresponds to the bound water in the structure. Two sharp peaks on the curve of $m/z$ 18 and $m/z$ 44 positioned at 300°C and 380°C are indicating combustion of residual organics and are producing weight loss of 5.65% and 5.63%, respectively. This reaction is associated with exothermic peaks on DSC curve. Above 400°C, slight weight gains of 0.03% to 500°C can be seen. The broad peak on the mass spectrum of $m/z$ 44 between 470°C and 530°C is connected with weight increase of 0.65%. It is correlated with third exothermic peak on DSC curve at 503°C. This may indicate that $\alpha$-$V_2O_5$-$\beta$-$V_2O_5$ phase transformation is associated with oxygen adsorption. Above 550°C to melting temperature (678°C), slight weight gain is visible again. This weight increase may be due to reoxidation of nonstoichiometric defects present in sample [22].

The infrared spectra of the powder samples after thermal treatment at different temperatures, 300°C, 350°C, 500°C, and 600°C, are illustrated in Figure 5.

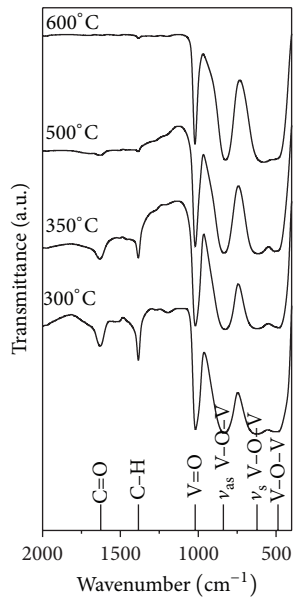


Figure 5: FT-IR spectra of samples after thermal treatment at different temperatures: 300°C, 350°C, 500°C, and 600°C.

The evidence for the structural determination of orthorhombic $V_2O_5$ crystals is the peak position of the vanadyl mode (vanadium oxygen double bond $\nu_s$ V=O) located at 1020 $cm^{-1}$ for all samples. Generally, the IR band of V=O in crystalline $V_2O_5$ is seen at 1017–1021 $cm^{-1}$. The sample annealed 300°C shows peak around 488 $cm^{-1}$ which is related to the bending vibration of the V–O–V bond. Moreover, the other two broad peaks at about 622 $cm^{-1}$ and 832 $cm^{-1}$ are attributed to the symmetric ($\nu_s$ V–O–V) and asymmetric stretching ($\nu_{as}$ V–O–V) of the V–O–V bond, respectively. The absorption peaks at 1384 $cm^{-1}$ and 1627 $cm^{-1}$ are due to scissoring of C–H and the stretching vibrations mode of C=O, respectively, which confirms the presence of residual organics in sample. Upon heating the

Table 1: Infrared peak positions and bond attributions in sample annealed at different temperatures and the comparison with the earlier literature reports.

| Bonding | IR peak positions ($cm^{-1}$) | | | | | | | Respective references |
|---|---|---|---|---|---|---|---|---|
| | Values obtained for powder samples heated at | | | | Literature values and annealing temperature | | | |
| | 300°C | 350°C | 500°C | 600°C | 170°C | 400°C | 600°C | |
| V–O–V bending | 488 | 488 | 497 | 495 | 450 | 476 | | [23, 24] |
| V–O–V stretching symmetric | 622 | 619 | 626 | 586 | 606 | 591 | 526 | [23–25] |
| V–O–V stretching asymmetric | 839 | 834 | 832 | 822 | 824 | 822 | 834 | [23–25] |
| V=O stretching symmetric | 1020 | 1020 | 1020 | 1020 | 1017 | 1018 | 1021 | [23–25] |
| C–H bending (scissoring) | 1384 | 1383 | 1383 | — | 1379 | | | [23] |
| C=O stretching | 1627 | 1650 | 1634 | — | 1633 | | | [23] |

sample up to 600°C significant change of IR spectrum is visible. Peaks attributed to organics impurities gradually disappeared with increasing temperature, indicating their elimination at 600°C. These results are consistent with TGA/MS data. Peaks observed in the region of 400–700 $cm^{-1}$ are assigned to symmetric stretching of V–O–V. It gradually shifts to the lower wave numbers and merges with bending V–O–V peak with increasing the annealing temperature to 600°C. FT-IR peaks position and bond attributions in samples and their comparison to the earlier literature are listed in Table 1 [23–25].

Figure 6 shows SEM images of the coatings deposited on quartz glass and silicon, obtained after thermal treatment at 200°C for 10 h (Figures 6(a) and 6(b), resp.). The structure seen in the pictures is homogenously porous, without any cracks. However based on SEM investigations it is not possible to clearly determine whether with increasing temperature from 100°C to 200°C the pore size changes and if the pore size is dependent on the substrate. Figures 6(c) and 6(d) show SEM of thin films deposited on quartz glass and silicon, respectively, heated at 300°C for 10 h. The SEM images show nanoclusters that were formed on the surface of the films.

The nanoclusters which were grown on the quartz glass and silicon have similar dimensions, independent of the kind of the substrate. The average diameter of the $V_2O_5$ nanoclusters grown on the samples is 500 nm–1000 nm. The effect of 480°C temperature annealing on the structure is presented in Figures 6(e) and 6(f). If to compare Figures 6(c) and 6(d) with Figures 6(e) and 6(f) it can be seen that this temperature induced a morphological transformation from nanoclusters to nanorods. When the temperature increased up to 480°C the rod-like structure of $V_2O_5$ was obtained on both substrates. Nanorods seen in Figures 6(e) and 6(f) have various sizes. The width of rods ranges between 200 nm and 700 nm, the length of 1 $\mu$m–6 $\mu$m and the thickness of nanorods ranges from 100 nm to 200 nm. With increasing annealing temperature to 600°C, films deposited on quartz glass and silicon got converted into $V_2O_5$ nanorods completely, and the dimensions of the nanorods became larger depending on the substrates (Figures 6(g) and 6(h), resp.). Nanorods grown on quartz glass substrate have irregular shape and various sizes, with length 3–10 $\mu$m and width 0.6 $\mu$m–2.5 $\mu$m. Nanorods growth on silicon substrate have more uniform size, with the length of 3 $\mu$m–5 $\mu$m and width between 500 nm and 1000 nm. The nanorods growth is due to oxygen adsorption, which is clearly seen on TGA curve (Figure 4) when weight increases at the temperature above 550°C. Summarizing SEM results it may be noticed that thermal treatment strongly influences crystallization process and as a result morphologies and crystal structures are highly dependent on the annealing temperature. This suggests that the surface diffusion phenomenon plays an important role in the growth process of nanorods. Since the annealing temperature is quite high, a high surface mobility is expected during the annealing process, thus favoring the nanorods growth [8, 15]. Actually, the surface diffusion phenomena are common during process of solid-state growth for elongated nanomaterials from initial nanoparticles or powders.

Figure 7 shows SEM images of powder samples annealed at different temperatures. The SEM images of xerogel powders annealed for 10 h at the temperatures from 100°C to 200 and 300°C reveal that samples have the same porous structure. Comparison to XRD results (Figure 2) may suggest that crystallization process at 300°C does not induce morphological changes. The effect of 350°C annealing temperature on the structure is presented in Figure 7(b). If to compare Figures 7(a) and 7(b) it can be seen that this temperature induced a morphological transformation from $V_2O_5$ pore structure to $V_2O_5$ nanostructured particles. This change is connected with exothermic peak on DSC curve (Figure 3) at 382°C. Besides, on the SEM images of the samples annealed at 350°C and 500°C (Figures 7(b) and 7(c), resp.), it is clear that the initial growth of $V_2O_5$ nanorods starts from the nanostructured particles. This significant morphological change is assigned to exothermic peak at 503°C on DSC curve and attributed to $\beta$-$V_2O_5$ phase formation. With increasing annealing temperature to 600°C, diameters and length of the $V_2O_5$ nanorods become larger (Figure 7(d)). The width of

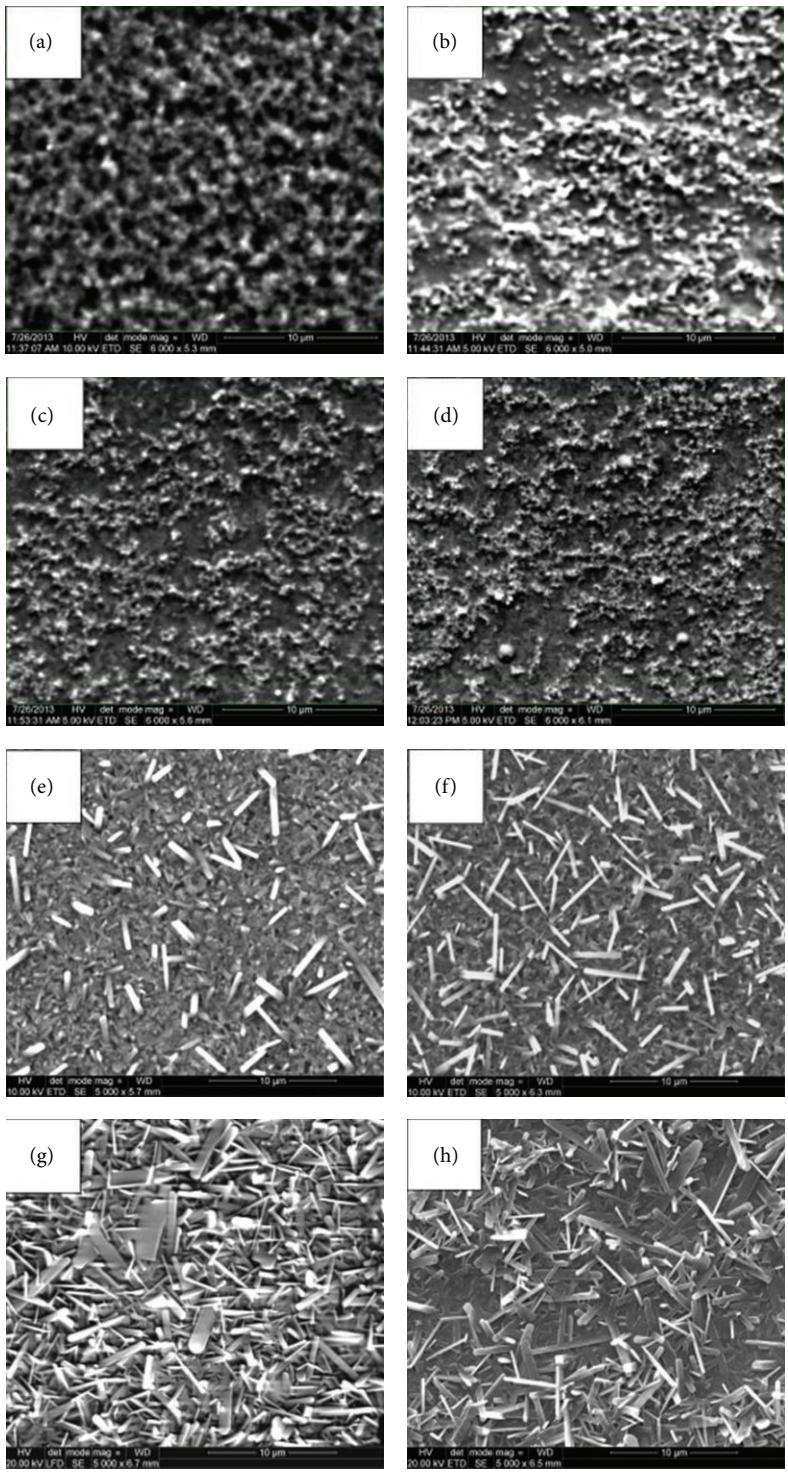


Figure 6: SEM images of the coatings annealed for 10 h at different temperatures. (a) 200°C, deposited on quartz glass, (b) 200°C, deposited on silicon, (c) 300°C, deposited on quartz glass, (d) 300°C, deposited on silicon, (e) 480°C, deposited on quartz glass, (f) 480°C, deposited on silicon, (g) 600°C, deposited on quartz glass, and (h) 600°C, deposited on silicon.

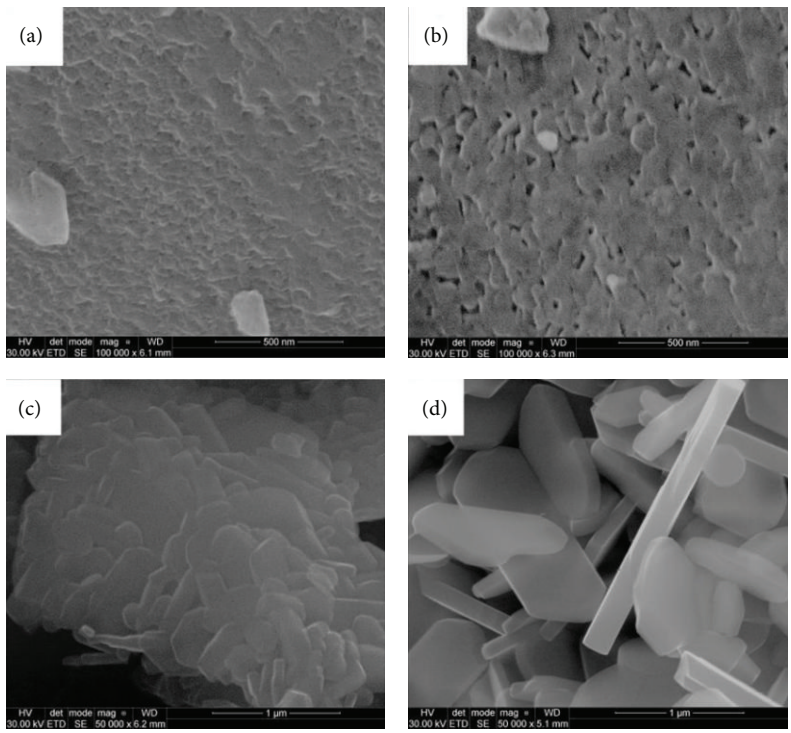


Figure 7: SEM images of the xerogel powders annealed for 10 h at different temperatures: (a) 300°C, (b) 350°C, (c) 500°C, and (d) 600°C.

rods ranges between 300 nm and 700 nm, the length 1 $\mu$m–2,5 $\mu$m and the thickness of nanorods is about 100 nm. The nanorods growth process in xerogel powder is similar to process described in case of thin films.

## 4. Conclusions

The crystallization process that occurs at different temperatures can be described as follows. The samples annealed at 100°C and 200°C are amorphous; with the increasing annealing temperature to 300°C, crystalline $V_2O_5$ nanoclusters are formed onto the surface of the films but did not have enough energy to form a crystal structure. A further increase in temperature up to 600°C causes nanorods growth. So it can be seen that thermal treatment strongly influences crystallization process and as a result morphologies and crystal structures are highly dependent on the annealing temperature. Additionally, a large impact on the size of nanorods has preparation method of the samples. The dimensions of nanorods which grown from xerogel powder and which grown on silicon substrate are similar. However, nanorods grown on quartz glass substrate are about 2–4 times longer and 2-3 times wider than nanorods grown from xerogel powder and grown on silicon substrate. It may be suggested that the type of substrate influences on nanorods dimension. In addition, the substrate stabilizes the structure and prevents transformation $\beta$-$V_2O_5$ into $\alpha$-$V_2O_5$ phase during cooling. In summary, the heat treatment of sol-gel derived material at 600°C leads to $V_2O_5$ nanorods crystallization with dimension depending on sample preparation method. This occurs both in sol-gel derived coatings and in the xerogel powders.

## Conflict of Interests

The authors declare that there is no conflict of interests regarding the publication of this paper.

## References

[1] D. L. da Silva, A. D. C. Viegas, J. J. J. Acuña, and A. A. Pasa, "Nanofiber-to-nanorod transformation during annealing of electrochemically deposited vanadium oxide nanofibers," *Materials Letters*, vol. 68, pp. 303–306, 2012.

[2] J. Cui, D. Da, and W. Jiang, "Structure characterization of vanadium oxide thin films prepared by magnetron sputtering methods," *Applied Surface Science*, vol. 133, no. 3, pp. 225–229, 1998.

[3] S. Chen, H. Ma, S. Wang et al., "Vanadium oxide thin films deposited on silicon dioxide buffer layers by magnetron sputtering," *Thin Solid Films*, vol. 497, no. 1-2, pp. 267–269, 2006.

[4] M. A. Kaid, "Characterization of electrochromic vanadium pentoxide thin films prepared by spray pyrolysis," *Egyptian Journal of Solids*, vol. 29, no. 2, pp. 273–291, 2006.

[5] S. H. S. Chan, T. Y. Wu, J. C. Juan, and C. Y. Teh, "Recent developments of metal oxide semiconductors as photocatalysts in advanced oxidation processes (AOPs) for treatment of dye waste-water," *Journal of Chemical Technology and Biotechnology*, vol. 86, no. 9, pp. 1130–1158, 2011.

[6] N. Özer, "Electrochemical properties of sol-gel deposited vanadium pentoxide films," *Thin Solid Films*, vol. 305, no. 1-2, pp. 80–87, 1997.

[7] R. Enjalbert and J. Galy, "A refinement of the structure of $V_2O_5$," *Acta Crystallographica*, vol. C42, no. 11, pp. 1467–1469, 1986.

[8] C. W. Zou, X. D. Yan, J. Han, R. Q. Chen, and W. Gao, "Microstructures and optical properties of $\beta$-$V_2O_5$ nanorods prepared by magnetron sputtering," *Journal of Physics D: Applied Physics*, vol. 42, no. 14, Article ID 145402, 2009.

[9] V. P. Filonenko, M. Sundberg, P.-E. Werner, and I. P. Zibrov, "Structure of a high-pressure phase of vanadium pentoxide, $\beta$-$V_2O_5$," *Acta Crystallographica Section B: Structural Science*, vol. 60, no. 4, pp. 375–381, 2004.

[10] A. Pan, J.-G. Zhang, Z. Nie et al., "Facile synthesized nanorod structured vanadium pentoxide for high-rate lithium batteries," *Journal of Materials Chemistry*, vol. 20, no. 41, pp. 9193–9199, 2010.

[11] T. Puangpetch, S. Chavadej, and T. Sreethawong, "Mesoporous-assembled $V_2O_5$ nanosheet synthesized via a surfactant-modified sol-gel technique and its photocatalytic $H_2$ production activity under visible light irradiation," *Powder Technology*, vol. 208, no. 1, pp. 37–41, 2011.

[12] S. Pavasupree, Y. Suzuki, A. Kitiyanan, S. Pivsa-Art, and S. Yoshikawa, "Synthesis and characterization of vanadium oxides nanorods," *Journal of Solid State Chemistry*, vol. 178, no. 6, pp. 2152–2158, 2005.

[13] D. di Claudio, A. R. Phani, and S. Santucci, "Enhanced optical properties of sol-gel derived $TiO_2$ films using microwave irradiation," *Optical Materials*, vol. 30, no. 2, pp. 279–284, 2007.

[14] J. Livage, F. Beteille, C. Roux, M. Chatry, and P. Davidson, "Sol-gel synthesis of oxide materials," *Acta Materialia*, vol. 46, no. 3, pp. 743–750, 1998.

[15] D. Vasanth Raj, N. Ponpandian, D. Mangalaraj, and C. Viswanathan, "Effect of annealing and electrochemical properties of sol-gel dip coated nanocrystalline $V_2O_5$ thin films," *Materials Science in Semiconductor Processing*, vol. 16, no. 2, pp. 256–262, 2013.

[16] M. Gotić, S. Popović, M. Ivanda, and S. Musić, "Sol-gel synthesis and characterization of $V_2O_5$ powders," *Materials Letters*, vol. 57, no. 21, pp. 3186–3192, 2003.

[17] M. Niederberger, M. H. Bartl, and G. D. Stucky, "Benzyl alcohol and transition metal chlorides as a versatile reaction system for the nonaqueous and low-temperature synthesis of crystalline nano-objects with controlled dimensionality," *Journal of the American Chemical Society*, vol. 124, no. 46, pp. 13642–13643, 2002.

[18] Q. Su, W. Lan, Y. Y. Wang, and X. Q. Liu, "Structural characterization of $\beta$-$V_2O_5$ films prepared by DC reactive magnetron sputtering," *Applied Surface Science*, vol. 255, no. 7, pp. 4177–4179, 2009.

[19] I. E. Wachs and B. M. Weckhuyesen, "Structure and reactivity of surface vanadium oxide species on oxide supports," *Applied Catalysis A: General*, vol. 157, no. 1-2, pp. 67–90, 1997.

[20] K. Honma, M. Yoshinaka, K. Hirota, O. Yamaguchi, J. Asai, and Y. Makiyama, "Fabrication, microstructure and electrical conductivity of $V_2O_5$ ceramics," *Materials Research Bulletin*, vol. 31, no. 5, pp. 531–537, 1996.

[21] A. Dhayal Raj, T. Pazhanivel, P. Suresh Kumar, D. Mangalaraj, D. Nataraj, and N. Ponpandian, "Self assembled $V_2O_5$ nanorods for gas sensors," *Current Applied Physics*, vol. 10, no. 2, pp. 531–537, 2010.

[22] J. Mendialdua, R. Casanova, and Y. Barbaux, "XPS studies of $V_2O_5$, $V_6O_{13}$, $VO_2$ and $V_2O_3$," *Journal of Electron Spectroscopy and Related Phenomena*, vol. 71, no. 3, pp. 249–261, 1995.

[23] A. Venkatesan, N. Krishna Chandar, S. Arjunan, K. N. Marimuthu, R. Mohan Kumar, and R. Jayavel, "Structural, morphological and optical properties of highly monodispersed PEG capped $V_2O_5$ nanoparticles synthesized through a non-aqueous route," *Materials Letters*, vol. 91, pp. 228–231, 2013.

[24] R. Abazari, S. Sanati, and L. A. Saghatforoush, "Non-aggregated divanadium pentoxide nanoparticles: a one-step facile synthesis. Morphological, structural, compositional, optical properties and photocatalytic activities," *Chemical Engineering Journal*, vol. 236, pp. 82–90, 2014.

[25] P. Ragupathy, S. Shivakumara, H. N. Vasan, and N. Munichandraiah, "Preparation of nanostrip $V_2O_5$ by the polyol method and its electrochemical characterization as cathode material for rechargeable lithium batteries," *Journal of Physical Chemistry C*, vol. 112, no. 42, pp. 16700–16707, 2008.